Ultrasensitive Gas-Phase Chemical Sensing Based on Functionalized Photonic Crystal Nanobeam Cavities

Yu Chen,[†,⊥] William S. Fegadolli,[‡,⊥] William M. Jones,[‡] Axel Scherer,[‡,§] and Mo Li[†,*]

[†]Department of Electrical and Computer Engineering, University of Minnesota, Minneapolis, Minnesota 55455, United States, [‡]Department of Physics, California Institute of Technology, Pasadena, California 91125, United States, and [§]Department of Electrical Engineering, California Institute of Technology, Pasadena, California 91125, United States. [⊥]Y. Chen and W. S. Fegadolli contributed equally to this work.

ABSTRACT Photonic crystal nanobeam cavities with high-quality factors are very sensitive to the changes of the dielectric properties of their surroundings. Utilizing this high sensitivity and by applying chemical functionalization, an ultrasensitive chemical sensor for gases based on a nanobeam cavity was demonstrated. A limit of detection of 1.5 parts-per-billion (ppb) in ambient conditions, determined from the noise level of the system, was achieved for nerve agent simulant methyl salicylate. The nanobeam cavity's nonlinear thermo-optical bistability is also utilized to realize a threshold detector for cumulative chemical exposure.

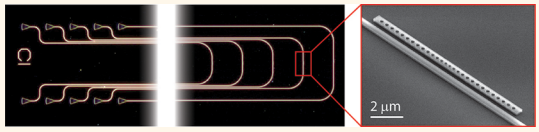

KEYWORDS: photonic crystal cavity · chemical sensor · thermo-optical bistability

Various types of photonic cavities and optical resonators based on dielectric materials with micro- or nanoscale dimensions have been developed, affording very high optical quality factors and finesse.[1] Those cavities can be categorized in two main types: whispering gallery resonators and photonic crystal cavities. While the highest quality factor achieved so far is obtained in whispering gallery resonators,[2] 2D and 1D photonic crystal cavities have the advantages of compactness, planar structures, design flexibility, and readiness for integration in photonic circuits. In particular, 1D photonic crystal nanobeam nanocavities have a very small footprint and can provide extremely high quality factors.[3,4] They are commonly fabricated on silicon-on-insulator (SOI) or silicon nitride on silicon substrates, which are compatible with CMOS (complementary metal–oxide–semiconductor) processes and thus can be fabricated in large scale at foundries. High-Q photonic crystal nanobeam cavities have been utilized in quantum optomechanics,[5] nanoparticle manipulation,[6] and nonlinear optics.[7]

With very high quality factors, the changes of the resonance frequencies of photonic cavities, which are susceptible to the change of the dielectric properties of the surrounding medium, can be resolved with very high precision. Generally, it is feasible to measure resonance wavelength shifts of 1/50–1/100 of the resonance line width.[8,9] Such a principle has been utilized to develop highly sensitive refractometric sensors based on various types of photonic cavities, capable of measuring refractive index change in the 10^{-4} to 10^{-6} range,[10−13] on a par with other optical techniques such as surface plasmonic resonance sensors and fiber grating sensors.[14,15] On a silicon photonics platform, previously a microring silicon optical resonator has been used to detect the presence and pressure of gaseous and liquid-phase chemicals.[13,16] Here we demonstrate the use of chemically functionalized nanobeam cavities as chemical sensors of analytes in gas phases.

Device Characterization. Figure 1a and b show, respectively, optical and scanning electron microscope images of a nanobeam cavity device used in this study. The nanobeam cavity is side coupled with a bus waveguide that has two integrated grating couplers for input and output of optical signals from and to optical fibers. The waveguide-loaded quality factors of as-fabricated devices were in the range 50 000–80 000.[17] To achieve selective and optimal chemiabsorption of specific types

* Address correspondence to moli@umn.edu.

Received for review September 27, 2013 and accepted December 3, 2013.

Published online December 03, 2013
10.1021/nn4050547

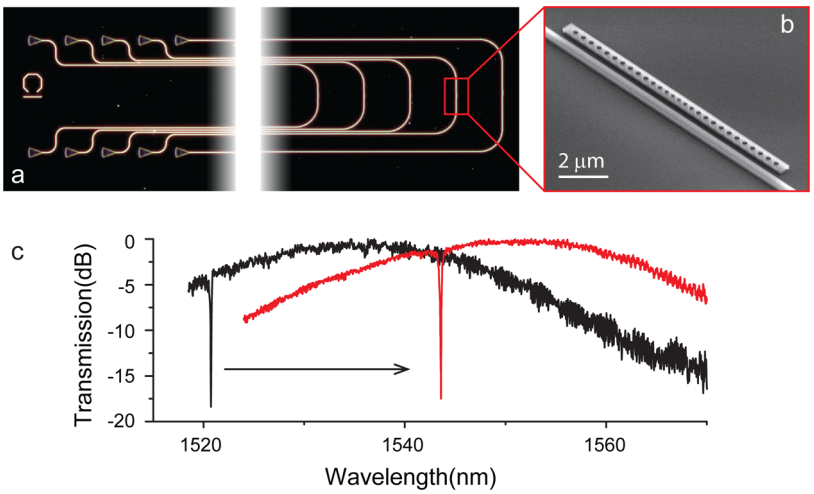

Figure 1. (a) Dark-field optical image of an array of nanobeam cavities coupled with waveguides and grating couplers. (b) Scanning electron microscope micrographic of a nanobeam photonic crystal cavity coupled to a bus waveguide. (c) Transmission spectra measured on the device with (red) and without (black) the polymer coating. The loaded quality factor has degraded from the as-fabricated value of 50 000 to 20 000 (black) after application and removal of the polymer coating, and 8000−10 000 (red) with the coating on the device.

of analytes, the nanobeam surface needed to be chemically functionalized. For homeland security applications, methyl salicylate (MeS) as a simulant of nerve agent gases was tested as the analyte gas in the sensing experiments. A fluoroalcohol polysiloxanes polymer (Adiol, Seacoast Scientific Inc.) was selected as the coating material for its strong and reversible bonding with MeS molecules, as well as its high thermal stability and stable interface with the substrate.[18] The polymer was used as purchased and dissolved in toluene to a volume concentration of 1 mg/mL. The solution was then spin coated on the device substrate at 3000 rpm for 30 s, and the substrate was baked on a hot plate at 90 °C for 1 min in ambient to evaporate the solvent. The process resulted in a layer of conformal polymer coating with a thickness in the range 60−80 nm on the nanobeam cavity. The thickness was measured by coating and patterning the polymer on a control sample and measuring the step height with an atomic force microscope. Coating with the polymer film induced a large red-shift of the resonance wavelength of the nanobeam cavity, as shown in Figure 1c. After the coating process, the loaded Q-factor of the devices was reduced to 8000−10 000. This significant drop in quality factors was attributed to the excess optical absorption in the polymer layer. Even after the removal of the coating and thorough cleaning, the loaded Q-factor recovered only to 20 000 (Figure 1c) due to residues of the polymer. To improve the device performance, it is thus desirable to select polymers with low optical absorption at near-infrared but high chemical specificity with targeted analytes. Using 3D FDTD simulation, the nanobeam cavity's response to the refractive index change of the polymer coating was determined to be more than 100 nm/RIU. Therefore, even after coating, the nanobeam cavities are capable of measuring refractive index change on the order of 10^{-5} in the polymer.

RESULTS

To measure optical resonance shift of the nanobeam cavity in response to the exposure of gaseous chemicals, we employed a simple slope detection method using a probe laser, as shown in Figure 2b. The laser wavelength was slightly blue-detuned from the resonance frequency, and the transmitted optical power was monitored with a photodetector. In this way, the shift of the resonance frequency was transduced to the change in the transmitted optical power. After calibrating the transmission spectrum of the system, the photodetector reading can be converted to resonance wavelength shift. Initially the probe laser power remained at a low level of 1 mW. Considering that the efficiency of the grating couplers is 20%, the intracavity energy is calculated to be ~2.7 femtojoules (or photon number $\sim 2 \times 10^4$). Because MeS has a dielectric constant larger than that of the Adiol polymer,[18] absorption of MeS into the polymer caused an increase (red-shift) of the resonance wavelength of the functionalized nanobeam cavity. Therefore, upon exposure to MeS gas, the transmission of the blue-detuned probe laser will increase. Figure 2c shows the measured responses when the device was exposed to MeS gas flow with varying volume concentration from 240 to 1200 parts-per-billion (ppb) for a period of 240 s in order to approach equilibrium state. In the gas generator, the analyte gas flow rate was kept at a constant value of 50 sccm, while the carrier gas flow rate was increased from 200 to 1200 sccm to gradually reduce the analyte concentration in the total flow during each test. It was confirmed in control experiments that changing the flow rate of the total gas flow containing

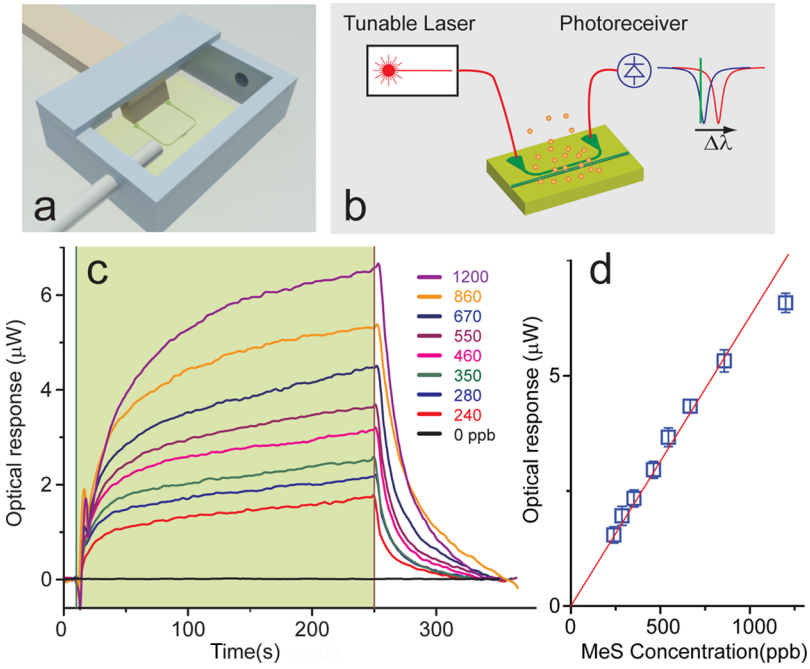

Figure 2. (a) Illustration of the measurement setup. A fiber array is used to couple light from optical fibers into grating couplers on the chip. A plastic chamber connected to the gas generator is used to enclose both the fiber array and the device chip. (b) Schematics of the optical measurement system based on the simple slope detection method. (c) The nanobeam's optical response to 240 s exposure (shaded area in light green) of MeS flow with varying volume concentrations, from low to high in eight steps, respectively: 240, 280, 350, 460, 550, 670, 860, 1200 ppb. The black trace is the system noise measured without any gas flow and using a 1 s integration time. (d) The nanobeam's optical response *versus* MeS concentration (symbols) along with a linear fit (red line). The system's limit of detection is determined to be 1.5 ppb by extrapolating to three times the system noise amplitude (black trace, panel c).

no analyte induced negligible responses of the device. In Figure 2c, the initial fast spike at the onset of analyte gas flow was attributed to the pressure shock when the flow valves inside the generator were switched to turn on the analyte flow and the consequent sudden temperature change at the device. The primary responses of the optical signal consist of fast and slow rising portions, which are very similar to the response of other types of polymer-coated chemical sensors, such as chemiresistors and chemicapacitors, and can be well modeled with Fick's equation of diffusion.[19] By fitting the fast portions of the responses at different concentration levels with the diffusion model, the diffusion constant of MeS in Adiol film was estimated to be about 1.4×10^{-13} cm^2/s. Thus for coating film thickness of 60 nm, the diffusion time is ~252 s; therefore the sensor's response is expected to approach equilibrium during the exposure time of 240 s. However, the measurement results show that it takes longer for the sensor's response to reach the equilibrium. This slow response is attributed to the large dead volume of the chamber and its large surface area where analyte can be absorbed onto, as well as the unpassivated walls of the tubing used in the experiment. All of these can be improved by optimal design of the sensor packaging and gas handling system, which are essential to gas-phase chemical sensors. Nevertheless, the nanobeam sensor has shown very high responsivity. Figure 2d shows that the device's response is linear to the analyte volume concentration with slight deviation at concentrations higher than 1 ppm, which is attributed to the reduced optical quality factor and the imprecision of the gas generator. In the form of resonance wavelength shift *versus* analyte concentration, the nanobeam's responsivity to MeS is measured to be 80 picometers/ppm. In Figure 2c, the system noise floor was measured using an averaging time of 1 s and zero MeS concentration in the gas flow. Using three times the rms amplitude (3σ) in the measured noise as the system noise floor, the limit of detection (LOD) in MeS concentration is determined to be 1.5 ppb, which is 1 order of magnitude lower than previously achieved values for MeS sensing using other chemical sensors.[18,20] We attribute the main contribution of the system noise to the fluctuation of the device's temperature, which, through thermo-optic effect, leads to fluctuation of the cavity's resonance frequency and is also affected by the gas flow rate. With a more advanced temperature stabilization scheme, the noise and consequently the sensitivity of the sensor can be significantly improved in future research.

Silicon has a relatively high thermo-optic coefficient of $1.86 \times 10^{(-4)}$/K, which causes a red-shift of the nanobeam cavity's resonance wavelength with increasing temperature. When the probe laser power was increased, the nanobeam cavities were heated primarily

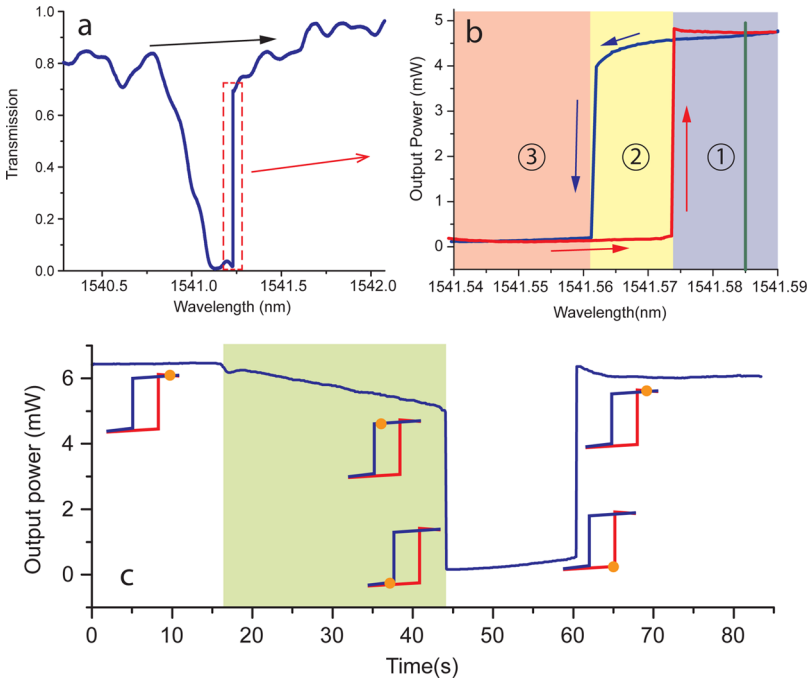

Figure 3. (a) Transmission spectrum of the nanobeam device measured using 8 dBm input laser power and by scanning the laser wavelength from low to high. The resonance peak is broadened with a sharp transition at the long wavelength side as the result of thermo-optic bistability. (b) Fine scan of probe laser wavelength in forward (red) and backward (blue) directions in the region near the transition between bistable states. The device shows two stable regions (1 and 3) and one bistable region (2). (c) The nanobeam sensor's response when it is operated in the bistable mode and exposed to MeS flow with a 1200 ppb concentration. The area in shaded green marks the duration of exposure. The orange circle in the symbols indicates the state of the device.

due to optical absorption in the polymer coating. The internal heating caused a thermo-optic bistability effect, as has been observed in many other types of optical cavities with high quality factors[21] and in our earlier work.[17] In Figure 3a, the transmission of the nanobeam was measured when the probe laser power of 8 dBm was used. Due to the thermally induced red-shift, the resonance peak was broadened as the laser wavelength was swept forward and a sudden transition happened when the laser wavelength surpassed the drifting resonance wavelength. In Figure 3b, the laser wavelength was swept in forward and then backward directions near the wavelength range where the transition happened. A clear bistability region (region 2) can be observed as a hysteresis loop between two stable regions (regions 1 and 3). Although often it is considered to be a nuance, we utilized this thermo-optic bistability to achieve a threshold mode of chemical sensing, which can trigger an alarm of a critical level of cumulative chemical exposure. We scanned the probe laser wavelength in the backward direction (following the blue trace in Figure 4b) and stopped at region 1 so that the device was at one of the stable states with a high level of transmitted power. When the resonance wavelength of the device shifted to longer wavelength, which was equivalent to scanning the probe laser wavelength backward, and beyond the lower bound of the bistable region 2 at ~1541.560 nm, the device swiftly switched to the lower stable state in region 3. The amount of the resonance wavelength shift for the transition to happen, which relates to the cumulative amount of analyte mass taken up by the polymer coating, is determined by the probe laser power level and wavelength. Thus, the position of the probe laser sets a threshold of the sensor's exposure to the targeted chemicals, beyond which a transition between the bistable states triggers an alarm. This process was observed in the experiments, and the result are shown in Figure 3c when the device was exposed to a 1200 ppb concentration of MeS. Initially the probe laser wavelength was set at 1541.585 nm and the device was at the stable state with high transmission in region 1. When the device was exposed to the analyte flow, its resonance wavelength gradually increased, causing a slow decrease in transmission along the blue trace in region 2. When more analyte molecules were absorbed by the polymer coating and the resonance wavelength shifted beyond the bistable threshold at ~1541.560 nm, the device switched to the lower stable state in region 3 with a low optical transmission. The analyte flow was then turned off. As the analyte molecules diffused out of the polymer and were purged, the resonance wavelength gradually recovered, following the red trace in Figure 3b from region 3 to 2 and eventually surpassed the upper bound of bistable region 2 and switched back to the stable state in region 1 with a high optical transmission.

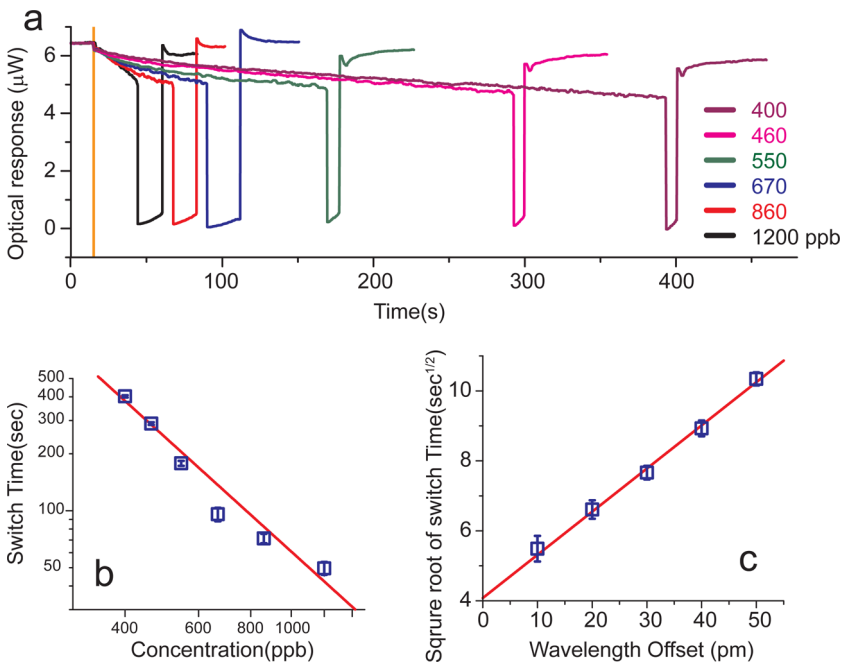

Figure 4. (a) The nanobeam sensor's response when it is operated in the bistable mode and exposed to MeS flow with concentration from low to high, respectively: 400, 460, 550, 670, 860, and 1200 ppb. The switching time decreases as the concentration increases. (b) Log−log plot of the switching time *versus* the MeS concentration, c_{gas} (symbols). Red line is a fitting with $1/c_{gas}^2$, showing excellent agreement. (c) Square root of switching time *versus* wavelength offset of the probe laser from the threshold wavelength of switching between two bistable states.

DISCUSSION

Assuming a constant diffusion coefficient, the switching time—the time that it takes from the turn-on of analyte flow to the switching between two bistable states—for given probe laser power and wavelength is determined by the concentration of analyte in the flow. As observed in the results in Figure 4a, the switching time increases when the analyte concentration in the flow is decreased. The switching time is the time for the given amount of analyte molecules to be taken up by the polymer film to shift the resonance wavelength to the threshold value (~1541.560 nm in Figure 3b). The absorption of an organic vapor into a polymer film can be described by Fick's equation of diffusion, and for low mass change of the polymer film, the mass taken up by the film after exposure time t is approximately given by[19]

$$M(t) = 2M(\infty)\left(\frac{Dt}{\pi h^2}\right)^{1/2} \quad (1)$$

where $M(\infty)$ is the analyte mass in the film at equilibrium, D is the diffusion coefficient of the analyte molecule in the polymer, and h is the thickness of the polymer film. The equilibrium analyte mass $M(\infty)$can be expressed as $M(\infty) = c_p V_p = K c_{gas} V_p$, where c_p and c_{gas} are the analyte volume concentration in the polymer film and in the gas flow, respectively, K is the partition coefficient at equilibrium, and V_p is the volume of the polymer film. Hence, the time it takes to absorb a threshold value of analyte mass M_{Th} in the polymer film can be expressed as

$$t_{Th} = \frac{\pi}{D}\left(\frac{M_{Th}(\lambda_p)}{2KA_p c_{gas}}\right)^2 = \frac{\pi}{D}\left(\frac{m_{Th}(\lambda_p)}{2Kc_{gas}}\right)^2 \quad (2)$$

where A_p is the surface area of the polymer film and m_{Th} is the threshold areal mass. Thus, the switching time t_{Th} is inversely proportional to the square of c_{gas}, the volume concentration of the analyte in the gas flow. In Figure 4b, the switching time is plotted *versus* the analyte concentration and fitted with $1/c_{gas}^2$, showing excellent agreement with eq 2. The result confirms that the nanobeam sensor can be accurately described by the simple diffusion model. The threshold mass, $m_{Th}(\lambda_p)$, is independent of c_{gas} but can be controlled by the probe laser wavelength: the closer the probe laser wavelength is set to the transition value, the less the amount of analyte needed to be absorbed to induce switching. In Figure 4c, the switching time measured at various probe laser wavelengths is plotted *versus* the wavelength offset from the switching threshold, the lower wavelength bound of the bistable region (~1541.56 nm in Figure 3b). A clear linear dependence of square root of the switching time on the wavelength offset can be observed, indicating a linear relation between the threshold mass and the wavelength offset. Thus, in this bistable mode, the nanobeam sensor can be utilized to detect a threshold level of analyte exposure. The threshold level is tunable by the probe laser wavelength and power and independent of the analyte gas concentration, so the

threshold mode is applicable to time varying concentration. It can find important applications in industrial and personal safety and production quality control.

CONCLUSION

In conclusion, we have demonstrated a CMOS-compatible photonic crystal nanobeam cavity functionalized with a fluoroalcohol polysiloxanes polymer to determine the concentration of MeS in the gas phase and to detect a threshold level of cumulative exposure. The proof-of-concept in this article demonstrates a versatile and highly integrated nanophotonic sensing platform that can be extended to detect other gas- and liquid-phase substances, simply by utilizing appropriate coating materials to achieve selective functionalization.

METHODS

The design of nanobeam cavities is described in detail in our earlier work.[17] In short, the reflector sections of the nanobeam cavity are designed with a periodic structure of nine holes, drilled through the silicon layer, with a periodicity of 0.9α (α = 453.2 nm). In addition, a linearly tapered section from the mirror section to the center of the cavity (from 0.5α to 0.395α) is designed with six holes to precisely phase match the waveguide and Bloch modes. A bus waveguide is used to couple light evanescently into the nanobeam cavity. The device was fabricated by means of a single step of electron beam lithography using a negative tone resist (HSQ), followed by reactive ion etching using a mixture of SF_6 and C_4F_8 gases.

The measurement setup used in this study is illustrated in Figure 2a. A commercial gas standard generation system (Kin-Tek 491M) was used to generate gas flow with precise analyte concentration using dry nitrogen as the carrier gas. In the generation system, a permeation tube containing liquid analyte and with an emission rate of 2340 ng/min at 100 °C was housed in a temperature-stabilized oven as the source of gaseous analyte. The emitted vapor of the analyte from the tube was diluted with the carrier gas with varying volume ratio to obtain the desired volume concentration. A plastic chamber connected to the outlet of the gas generator is used to enclose the device chip and the fiber array aligned with the input/output grating coupler to couple light into the bus waveguide. The relatively large volume of this chamber in order to accommodate the fiber array and the chip will reduce both the sensitivity and the response speed of the sensing system. If, instead, a miniaturized chamber integrated on the device chip, as demonstrated in ref 19, can be used, the performance of the device can be significantly improved. Nevertheless, very high sensitivity of the sensor has been demonstrated with the current primitive device packaging.

Conflict of Interest: The authors declare no competing financial interest.

Acknowledgment. This work is supported by the U.S. Army Research Office (Award No. W911NF-11-C-0052). M.L. also acknowledges funding support from the National Science Foundation (NSF CMMI-1162204). Parts of this work were carried out in the Kavli Nanoscience Institute at Caltech and the University of Minnesota Nanofabrication Center, which receives partial support from the NSF through the NNIN program, and the Characterization Facility, which is a member of the NSF-funded Materials Research Facilities Network *via* the MRSEC program.

REFERENCES AND NOTES

1. Vahala, K. J. Optical Microcavities. *Nature* **2003**, *424*, 839–846.
2. Lee, H.; Chen, T.; Li, J.; Yang, K. Y.; Jeon, S.; Painter, O.; Vahala, K. J. Chemically Etched Ultrahigh-Q Wedge-Resonator on a Silicon Chip. *Nat. Photonics* **2012**, *6*, 369–373.
3. Notomi, M.; Kuramochi, E.; Taniyama, H. Ultrahigh-Q Nanocavity with 1d Photonic Gap. *Opt. Express* **2008**, *16*, 11095–11102.
4. Quan, Q.; Deotare, P. B.; Loncar, M. Photonic Crystal Nanobeam Cavity Strongly Coupled to the Feeding Waveguide. *Appl. Phys. Lett.* **2010**, *96*, 203102.
5. Chan, J.; Alegre, T. P. M.; Safavi-Naeini, A. H.; Hill, J. T.; Krause, A.; Groblacher, S.; Aspelmeyer, M.; Painter, O. Laser Cooling of a Nanomechanical Oscillator into Its Quantum Ground State. *Nature* **2011**, *478*, 89–92.
6. Mandal, S.; Serey, X.; Erickson, D. Nanomanipulation Using Silicon Photonic Crystal Resonators. *Nano Lett.* **2009**, *10*, 99–104.
7. Pernice, W. H. P.; Xiong, C.; Schuck, C.; Tang, H. X. High-Q Aluminum Nitride Photonic Crystal Nanobeam Cavities. *Appl. Phys. Lett.* **2012**, *100*, 091105.
8. Vollmer, F.; Yang, L. Review Label-Free Detection with High-Q Microcavities: A Review of Biosensing Mechanisms for Integrated Devices. *Nanophotonics* **2012**, *1*, 267–291.
9. Lu, T.; Lee, H.; Chen, T.; Herchak, S.; Kim, J. H.; Fraser, S. E.; Flagan, R. C.; Vahala, K. High Sensitivity Nanoparticle Detection Using Optical Microcavities. *Proc. Natl. Acad. Sci. U.S.A.* **2011**, *108*, 5976–5979.
10. Dorfner, D. F.; Hurlimann, T.; Zabel, T.; Frandsen, L. H.; Abstreiter, G.; Finley, J. J. Silicon Photonic Crystal Nanostructures for Refractive Index Sensing. *Appl. Phys. Lett.* **2008**, *93*, 181103.
11. Yalcin, A.; Popat, K. C.; Aldridge, J. C.; Desai, T. A.; Hryniewicz, J.; Chbouki, N.; Little, B. E.; King, O.; Van, V.; Chu, S.; Gill, D.; Anthes-Washburn, M.; Unlu, M. S. Optical Sensing of Biomolecules Using Microring Resonators. *IEEE J. Sel. Top. Quantum Electron.* **2006**, *12*, 148–155.
12. De Vos, K.; Bartolozzi, I.; Schacht, E.; Bienstman, P.; Baets, R. Silicon-on-Insulator Microring Resonator for Sensitive and Label-Free Biosensing. *Opt. Express* **2007**, *15*, 7610–7615.
13. Iqbal, M.; Gleeson, M. A.; Spaugh, B.; Tybor, F.; Gunn, W. G.; Hochberg, M.; Baehr-Jones, T.; Bailey, R. C.; Gunn, L. C. Label-Free Biosensor Arrays Based on Silicon Ring Resonators and High-Speed Optical Scanning Instrumentation. *IEEE J. Sel. Top. Quantum Electron.* **2010**, *16*, 654–661.
14. Homola, J.; Yee, S. S.; Gauglitz, G. Surface Plasmon Resonance Sensors: Review. *Sens. Actuators, B* **1999**, *54*, 3–15.
15. White, I. M.; Fan, X. On the Performance Quantification of Resonant Refractive Index Sensors. *Opt. Express* **2008**, *16*, 1020–1028.
16. Robinson, J. T.; Chen, L.; Lipson, M. On-Chip Gas Detection in Silicon Optical Microcavities. *Opt. Express* **2008**, *16*, 4296–4301.
17. Fegadolli, W. S.; Oliveira, J. E.; Almeida, V. R.; Scherer, A. Compact and Low Power Consumption Tunable Photonic Crystal Nanobeam Cavity. *Opt. Express* **2013**, *21*, 3861–3871.
18. Patel, S. V.; Hobson, S. T.; Cemalovic, S.; Mlsna, T. E. Detection of Methyl Salicylate Using Polymer-Filled Chemicapacitors. *Talanta* **2008**, *76*, 872–877.
19. Charlesworth, J. M.; Partridge, A. C.; Garrard, N. Mechanistic Studies on the Interactions between Poly(pyrrole) and Organic Vapors. *J. Phys. Chem.* **1993**, *97*, 5418–5423.
20. Umasankar, Y.; Ramasamy, R. P. Highly Sensitive Electrochemical Detection of Methyl Salicylate Using Electroactive Gold Nanoparticles. *Analyst (Cambridge, U. K.)* **2013**, *138*, 6623–6631.
21. Almeida, V. R.; Lipson, M. Optical Bistability on a Silicon Chip. *Opt. Lett.* **2004**, *29*, 2387–2389.